Structural Uncoupling between Opposing Domains of Oxidized Calmodulin Underlies the Enhanced Binding Affinity and Inhibition of the Plasma Membrane Ca-ATPase†

Baowei Chen, M. Uljana Mayer, and Thomas C. Squier*

Cell Biology and Biochemistry Group, Biological Sciences Division, Pacific Northwest National Laboratory, P.O. Box 999, Richland, Washington 99352

Received December 9, 2004; Revised Manuscript Received January 12, 2005

ABSTRACT: Stabilization of the plasma membrane Ca-ATPase (PMCA) in an inactive conformation upon oxidation of multiple methionines in the calcium regulatory protein calmodulin (CaM) is part of an adaptive cellular response to minimize ATP utilization and the generation of reactive oxygen species (ROS) under conditions of oxidative stress. To differentiate oxidant-induced structural changes that selectively modify the amino-terminal domain of CaM from those that modulate the conformational coupling between the opposing domains, we have engineered a tetracysteine binding motif within helix A in the amino-terminal domain of calmodulin (CaM) that permits the selective and rigid attachment of the conformationally sensitive fluorescent probe 4′,5′-bis(1,3,2-dithioarsolan-2-yl)fluorescein-(1,2-ethanedithiol)$_2$ (FlAsH-EDT$_2$). The position of the FlAsH label in the amino-terminal domain provides a signal for monitoring its binding to the CaM-binding sequence of the PMCA. Following methionine oxidation, there is an enhanced binding affinity between the amino-terminal domain and the CaM-binding sequence of the PMCA. To identify oxidant-induced structural changes, we used frequency domain fluorescence anisotropy measurements to assess the structural coupling between helix A and the amino- and carboxyl-terminal domains of CaM. Helix A undergoes large amplitude motions in apo-CaM; following calcium activation, helix A is immobilized as part of a conformational switch that couples the opposing domains of CaM to stabilize the high-affinity binding cleft associated with target protein binding. Methionine oxidation disrupts the structural coupling between opposing globular domains of CaM, without affecting the calcium-dependent immobilization of helix A associated with activation of the amino-terminal domain to promote high-affinity binding to target proteins. We suggest that this selective disruption of the structural linkage between the opposing globular domains of CaM relieves steric constraints associated with high-affinity target binding, permitting the formation of new contact interactions between the amino-terminal domain and the CaM-binding sequence that stabilizes the PMCA in an inhibited conformation.

Calmodulin (CaM)[1] functions to mediate calcium signaling in all eukaryotes through the differential binding to more than 50 different target proteins, including kinases, phosphatases, ion channels, and pumps (*1*−*4*). Calcium ions bind to two EF-hand structures on each of the homologous domains; the four calcium binding sites are allosterically coupled through the central linker sequence (i.e., Met^{76} → Ser^{81}) connecting the opposing domains (Figure 1). Calcium binding is associated with domain activation through the dynamic stabilization of a defined conformation that exposes methionine-rich hydrophobic binding clefts (*5*−*9*). Following calcium activation, CaM is able to bind to a wide range of target proteins through mechanisms that normally involve

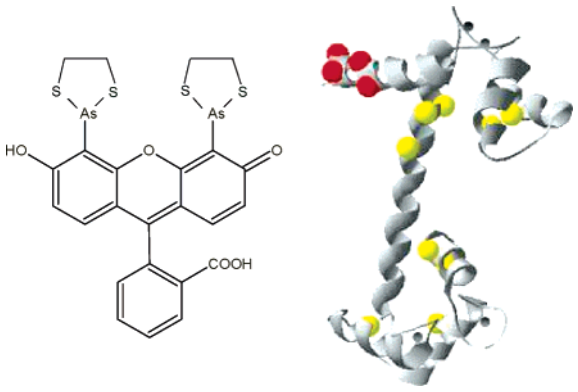

FIGURE 1: Structure of FlAsH-EDT$_2$ (left) and positions of the tetracysteine binding site (red) relative to nine methionines (yellow) in calcium-saturated CaM (right) using PDB entry 1cll (*73*). Bound calciums are shown as black circles.

† This work was supported by a grant from the National Institutes of Health (Grant AG17996) and by the U.S. Department of Energy, Office of Science Genomics:GTL project. Pacific Northwest National Laboratory is operated for the U.S. Department of Energy by Battelle Memorial Institute under Contract DE-AC06-76RLO 1830.

* To whom correspondence should be addressed: Pacific Northwest National Laboratory, P.O. Box 999, Mail Stop P7-53, Richland, WA 99352. E-mail: thomas.squier@pnl.gov. Telephone: (509) 376-2218. Fax: (509) 372-1632.

[1] Abbreviations: CaM, calmodulin; CaM$_{ox}$, oxidized calmodulin; EDTA, ethylenediaminetetraacetic acid; EGTA, ethylene glycol bis-(β-aminoethyl ether)-*N*,*N*,*N*′,*N*′-tetraacetic acid; FlAsH-EDT$_2$, 4′,5′-bis-(1,3,2-dithioarsolan-2-yl)fluorescein-(1,2-ethanedithiol)$_2$; HEPES, *N*-(2-hydroxyethyl)piperazine-*N*′-2-ethanesulfonic acid; KI, potassium iodide; β-ME, 2-mercaptoethanol; SDS−PAGE, sodium dodecyl sulfate−polyacrylamide gel electrophoresis; TCEP, tris(carboxyethyl)phosphine.

10.1021/bi0474113 CCC: $30.25
Published on Web 03/03/2005

the initial association between the C-terminal domain of CaM and the CaM-binding sequence of the target protein, followed by the structural collapse and binding of the amino-terminal domain (*10*−*14*).

The age-dependent selective oxidation of methionines in CaM functions to control cellular energy metabolism through the modulation of the binding mechanism to target proteins, including the plasma membrane Ca-ATPase (*15*−*19*). Following methionine oxidation in CaM, there is a large reduction in the ability of oxidized CaM (CaM_{ox}) to activate the plasma membrane Ca-ATPase with minimal effects on binding affinity (*20*). Irrespective of methionine oxidation, CaM binds to the same linear CaM binding sequence within the plasma membrane Ca-ATPase (*21*). However, bound CaM_{ox} is not displaced from the plasma membrane Ca-ATPase by unoxidized CaM, indicating differences in the binding interactions between the two globular domains and the binding sequence (*21*). These differences in binding are functionally important, since CaM_{ox} does not induce the structural transition within the binding sequence that is normally associated with enzyme activation, resulting in the downregulation of ATP utilization and cellular energy metabolism (*2*, *22*, *23*). Since methionine oxidation and the associated loss of CaM-dependent enzyme activation are reversible through the action of methionine sulfoxide reductase (*24*, *25*), these results suggest that methionine oxidation in CaM plays a regulatory role in modulating calcium signaling in response to oxidative stress.

Previous measurements have demonstrated global changes in the structure of CaM associated with methionine oxidation, which have been suggested to underlie the altered binding interaction between CaM and the plasma membrane Ca-ATPase as well as other target proteins (*15*, *21*, *26*). Furthermore, oxidized CaM binds and stabilizes the inhibitory domain of the plasma membrane Ca-ATPase in the inactive conformation (*22*, *23*). However, the underlying mechanisms responsible for observed reductions in the ability of CaM_{ox} to activate the plasma membrane Ca-ATPase and other target proteins are currently unclear. To clarify the relationships between (i) conformational changes associated with domain activation and the exposure of target protein binding sites and (ii) modulation of the structural coupling between the opposing globular domains, we have used site-directed mutagenesis to engineer a tetracysteine binding motif within helix A near the amino terminus of calmodulin (CaM) (Figure 1), permitting the selective and rigid attachment of the conformationally sensitive fluorescent probe 4′,5′-bis-(1,3,2-dithioarsolan-2-yl)fluorescein-(1,2-ethanedithiol)$_2$ (FlAsH-EDT_2). Measurements of the rate of FlAsH binding permit an assessment of the conformational dynamics of helix A, since FlAsH selectively associates with disordered peptide conformers (*27*), while complementary measurements of rotational motion of helix A using frequency domain fluorescence anisotropy permit a determination of the structural coupling between calcium activation and protein dynamics.

EXPERIMENTAL PROCEDURES

Materials. 4′,5′-Bis(1,3,2-dithioarsolan-2-yl)fluorescein-(1,2-ethanedithiol)$_2$ (FlAsH-EDT_2) was synthesized as previously described (*27*). The peptide C28W (LRRGQILWFRGLNRIQTQIRVVNAFRSS) was synthesized, purified, and confirmed by mass spectrometry to be greater than 95% pure by BioWORLD (Dublin, OH). Hydrogen peroxide (H_2O_2), *N*-(2-hydroxyethyl)piperazine-*N*′-2-ethanesulfonic acid (HEPES), tris(carboxyethyl)phosphine (TCEP), and potassium iodide (KI) were obtained from Sigma (St. Louis, MO). β-mercaptoethanol (β-ME) was obtained from Aldrich (Milwaukee, WI). Glycogen was obtained from ICN (Aurora, OH). All other chemicals were the purest grade commercially available.

Mutagenesis, Expression, and Purification of the CaM Mutant. DNA encoding the tetracysteine mutant of calmodulin encoding four cysteines at positions 6, 7, 10, and 11 was cloned into a pET-15b plasmid expression vector, and expressed in BL21(DE3) *Escherichia coli* cells, as previously described (*9*). Following expression, mutant CaM was purified by chromatography on phenyl-Sepharose CL-4B (Pharmacia, Piscataway, NJ), essentially as previously described (*28*, *29*). The protein concentration of CaM was measured using a micro-BCA assay reagent kit (Pierce, Rockford, IL), using desalted CaM as a protein standard [$\epsilon_{277} = 3029\ M^{-1}\ cm^{-1}$ (*28*, *30*)].

Polyacrylamide Gel Electrophoresis. Sodium dodecyl sulfate−polyacrylamide gel electrophoresis (SDS−PAGE) was performed according to the method of Laemmli (*33*). To detect calcium-dependent structure changes, either 10 mM $CaCl_2$ or 10 mM EDTA was added to the sample buffer, essentially as previously described (*34*). Protein bands were visualized with GelCode Blue Stain Reagent (Pierce).

Oxidation of CaM. All nine methionines within calmodulin were selectively oxidized, essentially as previously described (*25*, *31*). Briefly, 60 μM apo-CaM in 50 mM HEPES (pH 7.5) and 140 mM KCl (buffer A) was incubated for 24 h at 25 °C with 50 mM H_2O_2. The concentration of H_2O_2 was determined by using the published extinction coefficient [$\epsilon_{240} = 39.4 \pm 0.2\ M^{-1}\ cm^{-1}$ (*32*)]. The reaction was stopped by dialyzing against multiple changes of buffer A at 4 °C. Under these conditions, whole protein mass spectrometry has demonstrated that all nine methionines are quantitatively oxidized (*20*).

Labeling with FlAsH-EDT_2. Prior to addition of 1.0 μM FlAsH-EDT_2, the CaM mutant (1.0 μM) containing the tetracysteine motif in helix A, where E^6, E^7, A^{10}, and E^{11} were all mutated to cysteines (Figure 1), was incubated for 1 h at room temperature in 50 mM HEPES (pH 7.5), 140 mM NaCl, 1.0 mM β-mercaptoethanol, and 1.0 mM tris-(carboxyethyl)phosphine (TCEP) to reduce any disulfide bonds. Prior to fluorescence lifetime and anisotropy measurements, the mixture was incubated at 4 °C overnight. Gross structural changes were assessed using SDS−PAGE, which is commonly used to detect structural changes resulting from site-directed mutagenesis (*20*). The mobilities of the FlAsH-labeled CaM mutants were found to be similar to that associated with wild-type CaM (Figure 2), where oxidation of all nine methionines results in the same broadening of the CaM band on SDS−PAGE gels and a diminished calcium-dependent shift in mobility.

Steady-State Fluorescence Measurement. Fluorescence emission spectra of FlAsH−CaM were measured with a Fluoro Max-2 fluorometer (SPEX, Edison, NJ), using excitation and emission slits of 5 nm. In all cases, the sample

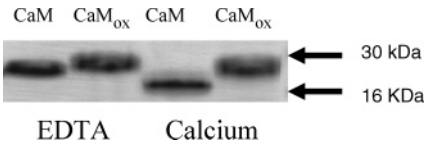

FIGURE 2: Diminished calcium-dependent shift in electrophoretic mobility upon methionine oxidation. Visualization on SDS−PAGE of tetracysteine mutants for unoxidized and oxidized CaM in the presence of either 10 mM EDTA or 10 mM $CaCl_2$. Arrows denote molecular mass standards and represent myoglobin (30 kDa) and lysozyme (16 kDa). In all cases, 5 μg of total protein was loaded onto the gel.

temperature was 25 °C, and the buffer consisted of 50 mM HEPES (pH 7.5), 140 mM NaCl, 1.0 mM β-mercaptoethanol, and 1.0 mM tris(carboxyethyl)phosphine (buffer A) in the presence of either a calcium chelator (either 1.0 mM EDTA or EGTA) or saturating calcium concentrations (i.e., 0.2 mM $CaCl_2$). Changes in the solvent accessibility of FlAsH were assessed through collisional quenching, where variable amounts of KI or acrylamide were added to 1.0 μM FlAsH−CaM. Data were analyzed as a function of the titrated quencher concentration and according to the Stern−Volmer equation:

$$F_0/F = 1 + K_{sv}[Q] = 1 + k_q\langle\tau\rangle[Q] \quad (1)$$

where F_0 and F are the fluorescence intensity in the absence and presence of added quencher, respectively, [Q] indicates the concentration of the quencher, KI, or acrylamide, and K_{sv} is the Stern−Volmer quenching constant, which is the product of both the average fluorescence lifetime in the absence of quencher ($\langle\tau\rangle$) and the bimolecular quenching constant (k_q) (*35*). The concentration of the C28W peptide was determined using the published extinction coefficient (ϵ_{280} = 5600 M^{-1} cm^{-1}) (*36*).

Determination of Binding Affinities. Peptide binding affinities for CaM were assessed using associated decreases in the fluorescence intensity of FlAsH−CaM upon peptide binding, essentially as previously described (*37*). This analysis assumes that there is a linear relationship between the decrease in the fluorescence signal and peptide binding, and that 1 mol of peptide binds 1 mol of CaM, as previously determined for C28W. Under these conditions, the amount of unbound (free) peptide can be calculated from the relative decrease in the fluorescence intensity, permitting a determination of the apparent binding constant (K_a) by assuming a simple binding isotherm (*38*), where

$$[C28W]_{bound} = [K_a[C28W]_{free}/(1 + K_a[C28W]_{free})] \times \text{span} + \text{minimum} \quad (2)$$

Span is related to the extent of peptide binding offset by a minimum value. Experimental data were fit using the Levenberg−Marquardt algorithm contained in ORIGIN (Microsoft Software, Inc., Northampton, MA).

Frequency Domain Fluorescence. The fluorescence lifetime and anisotropy were measured using an ISS (Urbana, IL) K2 fluorometer, whose design has previously been described in detail elsewhere (*39*, *40*). Excitation utilized the 488 nm output from a Coherent (Santa Clara, CA) Innova 400 argon ion laser; emitted light was collected after it had passed through a Schott OG-530 cutoff filter, using glycogen as a reference. All measurements were taken at 25 °C.

Analysis of Fluorescence Intensity and Anisotropy Decay. The frequency domain data were analyzed by a nonlinear least-squares method (*41*, *42*). The time-dependent decay $I(t)$ of fluorescence is generally fit to a sum of exponentials:

$$I(t) = \sum_{i=1}^{n} \alpha_i e^{-t/\tau_i} \quad (3)$$

where α_i values represent the pre-exponential factors, τ_i values represent the decay times, and n is the number of exponential components required to describe the decay. The intensity decay law is obtained from the frequency response of amplitude-modulated light and is characterized by the frequency-dependent values of the phase and the extent of demodulation. The values are compared with the calculated values from an assumed decay law until a minimum of the squared deviation (χ_R^2) is obtained. After the measurement of the intensity decay, the average lifetime was calculated:

$$\langle\tau\rangle = \frac{\sum_{i=1}^{n} \alpha_i \tau_i^2}{\sum_{i=1}^{n} \alpha_i \tau_i} = \sum_{i=1}^{n} f_i \tau_i \quad (4)$$

where f_i values represent the fractional intensities associated with each of the pre-exponential terms and $\langle\tau\rangle$ is directly related to the average time during which the fluorophore is in the excited state.

The frequency domain anisotropy decays $r(t)$ were fit to a multiexponential model:

$$r(t) = r_0 \sum_{i=1}^{n} g_i e^{-t/\phi_i} \quad (5)$$

where r_0 is the limiting anisotropy in the absence of rotational diffusion, φ_i values are the rotational correlation times, g_i represents the amplitude of the total anisotropy loss associated with each rotational correlation time, and n is the total number of components associated with the fluorescence decay (*43*). In all cases, parameter values are determined by minimizing the χ_R^2, which serves as a goodness-of-fit parameter that provides a quantitative comparison of the deviations between the measured and calculated values. Errors in the differential phase and modulated anisotropy were assumed to be 0.2° and 0.005, respectively.

RESULTS

Calcium-Dependent Mobility Shifts on SDS−PAGE. Calcium-dependent alterations in the electrophoretic mobility of CaM using SDS−PAGE have commonly been used to assess structural changes associated with calcium activation (*44*, *45*). Therefore, we have assessed the mobility of apo- and calcium-activated tetracysteine-CaM (Figure 2). We observe that upon calcium binding there is an increase in electrophoretic mobility analogous to that previously observed for wild-type CaM, which is indicative of normal conformational changes associated with calcium activation (*44*, *45*). These results indicate that the tetracysteine mutation does not significantly perturb the global protein fold and is consistent with prior measurements which demonstrated a

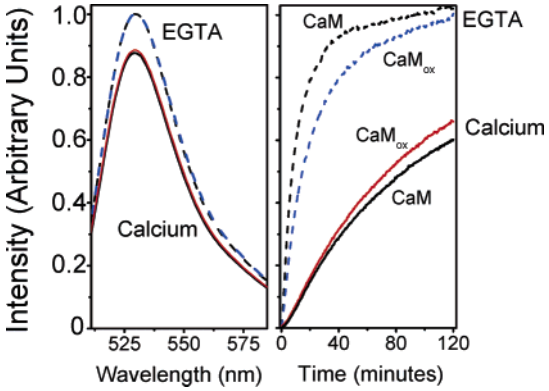

FIGURE 3: Differential FlAsH labeling of apo- and calcium-saturated CaM. Fluorescence emission spectra (left) and kinetics of FlAsH binding (right) to unoxidized (black) or oxidized (red and blue) apo-CaM (dashed lines) or following calcium activation (solid lines). Experimental conditions included 1.0 μM CaM in 50 mM HEPES (pH 7.5), 140 mM NaCl, 1.0 mM β-mercaptoethanol, and 1.0 mM tris(carboxyethyl)phosphine in the presence of either 1.0 mM EGTA (dashed lines) or 0.2 mM $CaCl_2$ (solid lines) at 25 °C. Excitation was at 500 nm, and fluorescence emission was measured at 530 nm.

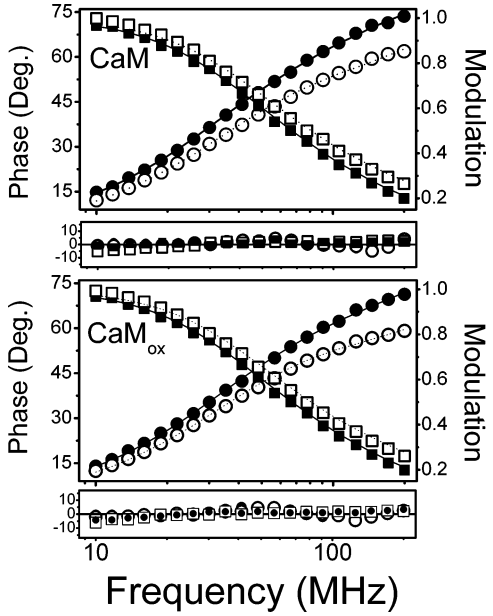

FIGURE 4: Lifetimes of FlAsH are unaffected by methionine oxidation. The frequency response and associated nonlinear least-squares fits to a two-exponential decay for the phase shift (○ and ●) and modulation (□ and ■) for FlAsH covalently bound to helix A for the apo- (● and ■) and calcium-saturated (○ and □) form of native (top) or oxidized (bottom) CaM. Weighted residuals (shown below the data) correspond to the difference between the experimental data and the calculated fit divided by the standard error of the individual measurement, assumed to be 0.2° and 0.005 for phase and modulation data, respectively. Experimental conditions included 1.0 μM CaM in 50 mM HEPES (pH 7.5), 140 mM NaCl, and either 1.0 mM EGTA or 0.2 mM $CaCl_2$ at 25 °C. Excitation was at 488 nm, and fluorescence emission was collected after the light had passed through a Schott OG-530 cutoff filter.

retention of function following mutation with no change in either apparent affinity or maximal levels of enzyme activation (*9*). Upon oxidation of all nine methionines, there is an altered mobility that is relatively insensitive to calcium binding, as previously documented following the methionine oxidation of wild-type CaM (*16*, *20*, *34*). Under these conditions, CaM retains the ability to bind all four calcium ligands (*15*, *46*), indicating that differences in the calcium-dependent change in electrophoretic mobility are probably related to the reduced conformational stability of oxidized CaM.

Fluorescence of FlAsH-Labeled CaM. To address the underlying conformational changes associated with oxidation of CaM, we have used FlAsH-EDT_2 to label the tetracysteine motif in helix A of CaM (Figure 1). FlAsH-labeled CaM retains the ability to fully activate target proteins, with essentially no change in either the apparent affinity or maximal extent of enzyme activation of phosphodiesterase (*9*). Furthermore, the mobility of the FlAsH-labeled CaM on SDS−PAGE gels is equivalent to that of wild-type CaM both prior to and following methionine oxidation (data not shown), indicating that the backbone fold is unaffected by the probe. The resulting adduct has an emission maximum near 530 nm that is insensitive to the oxidation of all nine methionines (Figure 3A). Further, irrespective of the oxidation of methionines in CaM, there is a 12−13% decrease in the fluorescence intensity upon calcium binding that is indicative of global conformational changes associated with the calcium activation of CaM. Similar results are apparent using frequency domain fluorescence spectroscopy to measure the fluorescence excited-state lifetimes of FlAsH-labeled CaM, which provide additional resolution of possible changes in the polarity and solvent exposure of the FlAsH chromophore (Figure 4). The extent of the phase shift and modulation decrease are inversely related to the lifetime of the fluorophore, where a shift in the frequency response to higher frequencies is indicative of a shorter average excited-state lifetime. In comparison to apo-CaM, the frequency response of calcium-activated CaM is shifted to higher frequencies that is indicative of a shorter excited-state lifetime. Virtually identical frequency responses are observed for native and oxidized CaM, indicating that methionine oxidation does not affect the fluorescence lifetime decay of FlAsH bound to helix A. In all cases, a nonlinear least-squares fit to the data can be described by a sum of two exponentials, as indicated by the random distribution of the weighted residuals (Figure 4 and Table 1). Thus, irrespective of methionine oxidation, there is a 17 ± 3% decrease in the average fluorescence lifetime of FlAsH bound to CaM upon calcium activation that is reflected in decreases in each of the individual lifetime components (τ_i); similar differences are observed in the contributing amplitudes (α_i) upon calcium activation irrespective of methionine oxidation that are indicative of similar local changes in the environments around FlAsH in apo- and calcium-activated CaM irrespective of methionine oxidation.

Conformational Changes in Helix A. Large increases in the quantum yield of FlAsH upon binding to tetracysteine motifs in proteins permit the ready determination of the kinetics of labeling, which has previously been demonstrated to be dependent on secondary structure, where greater helical propensity and conformational order result in a diminished rate of labeling (*27*). One observes that there are large differences in the kinetics of labeling for apo- and calcium-activated CaM, where calcium activation results in a large decrease in the rate of labeling (Figure 3B). Since the FlAsH probe binds selectively to the disordered tetracysteine motif, these results indicate that calcium binding stabilizes helix A. The initial rates of labeling helix A with FlAsH-EDT_2 following calcium activation are virtually identical, irrespec-

Table 1: Lifetime Data and Solvent Accessibility for FlAsH-Labeled CaM[a]

ligand	sample	α_1	τ_1 (ns)	α_2	τ_2 (ns)	$\langle\tau\rangle$[b] (ns)	k_q[c] ($\times 10^{-8}$ M^{-1} s^{-1}) KI	k_q[c] ($\times 10^{-8}$ M^{-1} s^{-1}) acrylamide
EGTA	CaM	0.34 ± 0.01	1.2 ± 0.2	0.66 ± 0.01	4.5 ± 0.1	4.1 ± 0.1	2.4 ± 0.2	ND[d]
	CaM_{ox}	0.37 ± 0.02	1.0 ± 0.2	0.63 ± 0.02	4.4 ± 0.1	4.0 ± 0.1	2.4 ± 0.1	ND[d]
Ca^{2+}	CaM	0.52 ± 0.02	0.8 ± 0.1	0.48 ± 0.02	4.0 ± 0.1	3.4 ± 0.1	2.2 ± 0.1	0.89 ± 0.04
	CaM_{ox}	0.55 ± 0.04	0.6 ± 0.1	0.45 ± 0.04	3.8 ± 0.2	3.3 ± 0.2	3.0 ± 0.4	1.33 ± 0.09
C28W	CaM	0.75 ± 0.06	0.5 ± 0.1	0.25 ± 0.06	3.6 ± 0.2	2.7 ± 0.3	ND[d]	1.5 ± 0.2
	CaM_{ox}	0.83 ± 0.08	0.4 ± 0.1	0.17 ± 0.08	3.4 ± 0.3	2.2 ± 0.4	ND[d]	2.5 ± 0.5

[a] Average pre-exponential terms (α_i) and lifetimes (τ_i) obtained from two-exponential fits to frequency domain data for the time-dependent intensity decay, $I(t)$, for FlAsH covalently bound to Cys^6, Cys^7, Cys^{10}, and Cys^{11} engineered into helix A of CaM, assuming $I(t) = \sum_i \alpha_i \exp(-t/\tau_i)$. [b] $\langle\tau\rangle = \sum_i \alpha_i\tau_i^2/\sum_i \alpha_i\tau_i$. Errors represent the standard errors of the mean for three independent measurements. [c] Bimolecular quenching constants (k_q) determined from the slopes in Figures 7 and 8. Experimental conditions include 1.0 μM FlAsH−CaM in 50 mM HEPES (pH 7.5), 140 mM NaCl, 1.0 mM β-mercaptoethanol, 1.0 mM TCEP, and either 1.0 mM EGTA (EGTA), 0.2 mM $CaCl_2$ (Ca^{2+}), or 3.0 μM C28W at 25 °C. [d] Not determined.

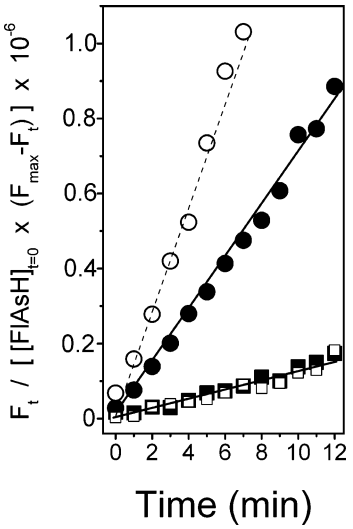

FIGURE 5: Initial rates of FlAsH binding for oxidized (● and ■) or wild-type (○ and □) CaM in the apo state (○ and ●) or following calcium activation (□ and ■). Rates of reaction were determined to be 2830 ± 80 M^{-1} s^{-1} (○, apo-CaM), 310 ± 10 M^{-1} s^{-1} (□, Ca_4-CaM), 1160 ± 30 M^{-1} s^{-1} (●, apo-CaM_{ox}), and 313 ± 8 M^{-1} s^{-1} (■, Ca_4-CaM_{ox}). Rate constants were calculated from the data in Figure 3, taking into account the fact that the reaction between FlAsH-EDT_2 and CaM resulting in fluorescence is a second-order reaction (*9*, *27*). If the fact that the concentrations of reactants (i.e., FlAsH-EDT_2 and CaM) are identical at zero time is taken into account, the general rate law simplifies to $F_t/[[\text{FlAsH-EDT}_2]_{t=0} \times (F_{max} - F_t)] = kt$, where F_{max} is the fluorescence maximum, F_t is the fluorescence at time t, $[\text{FlAsH-EDT}_2]_{t=0}$ is the concentration of FlAsH-EDT_2 at time zero, k is the second-order rate constant, and t is the time of reaction (*74*−*76*).

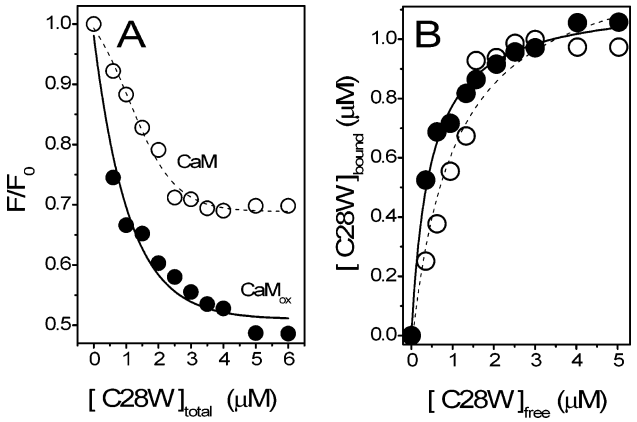

FIGURE 6: Methionine oxidation enhances association with the CaM-binding sequence of plasma membrane Ca-ATPase. Association of FlAsH−CaM with C28W, the binding sequence of the plasma membrane Ca-ATPase, results in a decrease in the fluorescence quantum yield (left) that permits the calculation of the binding isotherm (right) for the association of the amino-terminal domain of wild-type (○) and oxidized (●) CaM with C28W. Lines represent nonlinear least-squares fits to eq 2, where K_a equals 0.9 ± 0.2 μM^{-1} for wild-type CaM and 2.3 ± 0.5 μM^{-1} for CaM_{ox}. Experimental conditions included 1.0 μM CaM in 50 mM HEPES (pH 7.5), 140 mM KCl, and 0.2 mM $CaCl_2$ at 25 °C. Excitation was at 500 nm, and fluorescence emission was measured at 530 nm.

tive of the oxidation of methionines (Figure 5). However, there are significant differences in the rates of FlAsH binding to apo-CaM in response to methionine oxidation; the rate of binding is reduced by approximately 60% following oxidation of all nine methionines. The reduced rate of FlAsH binding to apo-CaM is indicative of a more stable helical structure following methionine oxidation in comparison to unoxidized apo-CaM.

Binding Affinity of the Amino-Terminal Domain. There is a significant decrease in the fluorescence intensity upon association of FlAsH−CaM with the CaM-binding sequence (i.e., C28W) of the plasma membrane Ca-ATPase (Figure 6A), permitting an assessment of how oxidation alters the affinity of the amino-terminal domain of CaM. In the case of unoxidized CaM, there is a $31 \pm 1\%$ decrease in the fluorescence intensity associated with binding C28W; the half-point of the titration requires a molar ratio of 1.4 ± 0.1 mol of C28W per mole of CaM. Following oxidation of all nine methionines, there is a $49 \pm 2\%$ decrease in fluorescence intensity upon binding C28W, with a half-point of binding at 0.8 ± 0.1 mol of C28W per mole of CaM_{ox}. The greater decrease in fluorescence intensity associated with CaM_{ox} binding to C28W is indicative of an altered binding conformation of the amino-terminal domain of CaM_{ox} in complex with C28W that is consistent with the nonproductive binding and diminished activity of CaM_{ox} in complex with the plasma membrane Ca-ATPase (*21*). The reduction in the concentration of C28W necessary for 50% binding indicates a higher binding affinity following oxidation of all nine methionines, suggesting that oxidation stabilizes the high-affinity binding cleft in the amino-terminal domain of CaM_{ox}. Assuming a linear relationship between the decrease in fluorescence and binding, it is apparent that the association constant is increased by approximately 2-fold upon oxidation of all nine methionines in CaM, from 0.9 ± 0.2 μM^{-1} for wild-type CaM to 2.3 ± 0.5 μM^{-1} for oxidized CaM (Figure 6B).

Solvent Accessibility of FlAsH. To better understand the conformational changes around helix A induced by methio-

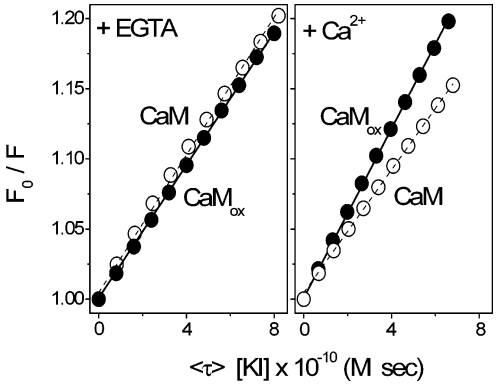

FIGURE 7: Minimal changes in solvent accessibilities of FlAsH−CaM upon methionine oxidation. Modified Stern−Volmer plots of the quenching of FlAsH bound to apo- (left) or calcium-activated (right) CaM prior to (○) or following oxidation of all nine methionines (●). Experimental conditions included 1.0 μM FlAsH-labeled CaM in 50 mM HEPES (pH 7.5), 140 mM NaCl, and either 1.0 mM EGTA or 0.2 mM $CaCl_2$ at 25 °C. Excitation was at 500 nm, and fluorescence emission was measured at 530 nm.

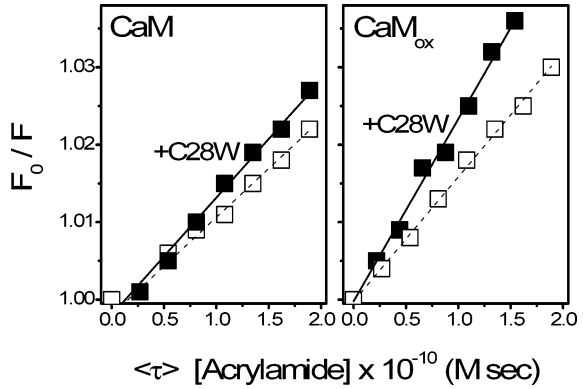

FIGURE 8: Increased solvent accessibility of FlAsH−CaM upon peptide binding. Modified Stern−Volmer plots of the acrylamide quenching of FlAsH bound to CaM for the wild-type (left) or oxidized (right) form in the absence (□) and presence (■) of bound C28W, a peptide corresponding to the CaM-binding sequence of the plasma membrane Ca-ATPase. Experimental conditions included 2.0 μM FlasH-labeled CaM in 50 mM HEPES (pH 7.5), 140 mM KCl, 0.2 mM $CaCl_2$, and, when indicated, 8.0 μM C28W at 25 °C. Excitation was at 500 nm, and fluorescence emission was measured at 530 nm.

nine oxidation, we have measured the solvent accessibility of FlAsH. In these measurements, the bimolecular quenching constant (k_q) is obtained from the slope of the change in fluorescence intensity upon varying the concentration of collisional quencher iodide in a modified Stern−Volmer quenching plot for either CaM alone or following association with the CaM-binding sequence of the plasma membrane Ca-ATPase (see eq 1 in Experimental Procedures). A comparison of the solvent accessibility of unoxidized and oxidized CaM indicates that upon oxidation of all nine methionines there is no change in the solvent exposure of FlAsH in helix A in apo-CaM; in comparison to that of native CaM, there is a 40 ± 20% increase in solvent accessibility of CaM_{ox} following calcium activation (Figure 7). A similar 50 ± 10% increase in solvent accessibility is observed using the noncharged collisional quencher acrylamide (Table 1).

The effects of peptide binding on CaM structure were measured by considering changes in the solvent accessibilities of FlAsH for calcium-activated CaM upon binding to the CaM-binding sequence of the plasma membrane Ca-ATPase (i.e., C28W). Upon binding to C28W, there is a 70−80% increase in the solvent accessibility of FlAsH bound to helix A relative to calcium-activated CaM, irrespective of methionine oxidation (Figure 8). These results indicate that similar structural rearrangements are associated with the formation of a high-affinity binding interface, but that oxidation induces a distinct structure that is maintained upon association with target peptides. These results indicate that the amino-terminal domain of CaM_{ox} assumes an altered conformation, which may underlie the nonproductive association between oxidized CaM and the plasma membrane Ca-ATPase.

Helix A Dynamics. Frequency domain fluorescence anisotropy measurements of the rotational dynamics of helix A permit an understanding of how oxidation modulates the structural coupling between the high-affinity calcium binding sites and the stabilization of binding clefts associated with target protein activation. Previous measurements demonstrated that upon calcium activation, helix A becomes motionally restricted as a result of stabilizing interactions with helix D, which mediates the structural coupling between the opposing domains of CaM and functions to stabilize the binding cleft associated with target protein association (*9*, *47*). To assess how oxidation affects helix A dynamics, the differential phase and modulated anisotropy of FlAsH bound to apo- and calcium-activated CaM were collected over 20 frequencies between 20 and 200 MHz (Figure 9). One observes similar frequency responses for the differential phase and modulated anisotropy irrespective of methionine oxidation. For apo-CaM, the differential phase increases from 3° at 10 MHz to a maximum of approximately 8° at 60 MHz. In contrast, a much smaller change in the differential phase is observed following calcium activation, which increases from 2° at 10 MHz to a maximum of 4.6° at 50 MHz.

A qualitative interpretation of these results is apparent if one remembers that the modulation frequency is inversely related to the rate of motion such that high and low frequencies correspond to fast and slow rates of motion, respectively. Further, the modulated anisotropy observed at long times (i.e., 10 MHz) is a reflection of the residual anisotropy that is related to the amplitude of helix A motion, while that observed at short times (i.e., 200 MHz) provides an indication of the initial anisotropy that is related to the extent of the resolved fluorescence anisotropy decay. Likewise, faster rates of motion result in larger changes of the differential phase at lower modulation frequencies. Thus, the reduction in the maximal change in the differential phase following calcium activation is indicative of a calcium-dependent immobilization of helix A. The very similar frequency responses observed for native and oxidized CaM indicate that the oxidation of all nine methionines in CaM does not affect the calcium-dependent stabilization of helix A associated with the formation of a high-affinity binding cleft for target protein binding.

A nonlinear least-squares fit of the data to determine the rates and amplitudes of helix A motion provides a quantitative understanding of oxidation-induced changes in the structure of CaM. Irrespective of methionine oxidation, the fluorescence anisotropy decays for apo-CaM are described by two rates of motion, corresponding to the motion of helix A (φ_1 = 1.2 ns) and a longer rotational correlation time associated with the hydrodynamic properties of the amino-

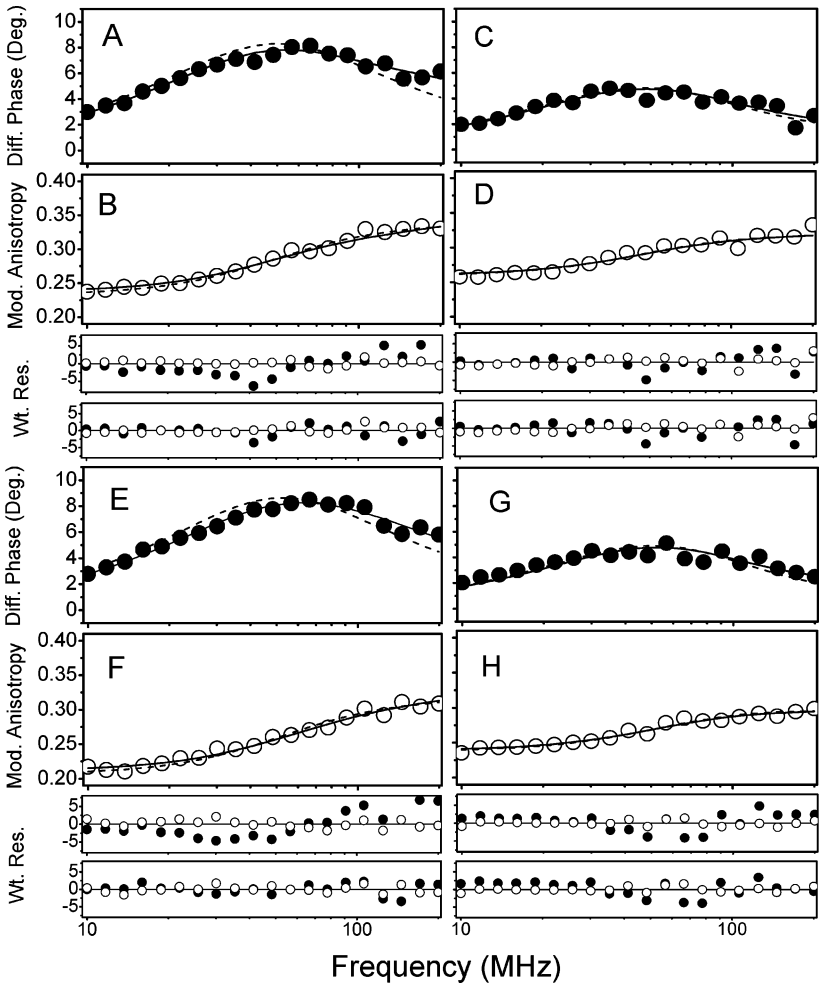

FIGURE 9: Calcium-dependent changes in the rotational dynamics of helix A are retained following methionine oxidation. Calcium-dependent changes in the rotational dynamics of FlAsH-labeled CaM and CaM_{ox} were measured using frequency domain fluorescence spectroscopy. Differential phase angles (●) and modulated anisotropy (○) were measured for 1.0 μM wild-type (A−D) or oxidized CaM (E−H) in 50 mM HEPES (pH 7.5), 140 mM NaCl, and either 1.0 mM EGTA (left panels) or 0.2 mM $CaCl_2$ (right panels) at 25 °C. Nonlinear least-squares fits are illustrated for models corresponding to a single rotational rate (dashed line) or two rotational rates (solid line). Weighted residuals (Wt. Res.), corresponding to the experimental data minus the calculated value normalized by the standard error of the measurement, are illustrated below each measurement of the differential phase and modulated anisotropy for models involving a single-exponential (top) and two-exponential (bottom) decay. Errors in the measurement of the differential phase and modulated anisotropy were assumed to be 0.2° and 0.005, respectively. Excitation was at 488 nm, and fluorescence emission was collected after the light had passed through a Schott OG-530 cutoff filter.

Table 2: Rotational Dynamics of FlAsH−CaM[a]

ligand	sample	g_1	ϕ_1 (ns)	g_2	ϕ_2 (ns)	χ_R^2
EGTA	CaM	0.10 ± 0.04	1.1 ± 0.5	0.90 ± 0.03	10 ± 1	4.3
	CaM_{ox}	0.12 ± 0.02	1.2 ± 0.3	0.88 ± 0.03	9 ± 1	3.1
Ca^{2+}	CaM	−	−	1.0	15 ± 2	5.1
	CaM_{ox}	−	−	1.0	11 ± 1	4.6

[a] Indicated values are for the pre-exponential amplitudes (i.e., g_i) and rotational correlation times (i.e., φ_i) with associated standard errors of the mean obtained from three independent measurements of the anisotropy decay, $r(t)$, which equals $r_o \sum_i g_i \exp(-t/\varphi_i)$. The limiting anisotropy (i.e., r_0) was 0.34 ± 0.04. The goodness of fit (i.e., χ_R^2) was calculated assuming frequency-independent errors in the differential phase and modulated anisotropy, which were assumed to be 0.2° and 0.005, respectively. Experimental conditions are as described in the legend of Figure 9.

terminal domain ($\varphi_2 = 10$ ns) (Table 2). The preexponential term (i.e., g_1) associated with the independent motion of helix A is not significantly changed upon oxidation of all nine methionines, indicating that there is a similar amplitude of motion, which corresponds to a full cone angle of approximately 30° (*48*−*50*). Following calcium activation, a single longer rotational correlation time fully describes the anisotropy decay for calcium-activated CaM (Table 2), as judged by the randomly weighted residuals (Figure 9). Thus, following calcium activation, helix A is structurally coupled to the entire CaM molecule. However, while the observed rotational correlation time of unoxidized CaM ($\varphi_2 = 15 \pm 2$ ns) agrees with the hydrodynamic calculations for the overall rotational dynamics of calcium-activated CaM using the structure in Figure 1 (i.e., $\varphi_r = {}^1/_6 Dr = 15.7$ ns) (*51*, *52*); following oxidative modification of all nine methionines, the rotational correlation time approximates that associated with that of the amino-terminal domain (i.e., $\varphi_2 = 11 \pm 1$ ns) as judged by the lack of overlap in the error surfaces in a rigorous analysis of correlated errors in the fit to the data (*53*) (Figure 10).

Taken together, these results indicate that methionine oxidation induces no change in the considerable dynamic flexibility for helix A, and by implication the amino-terminal domain, in apo-CaM. Following calcium activation, helix A is immobilized as part of a structural transition associated

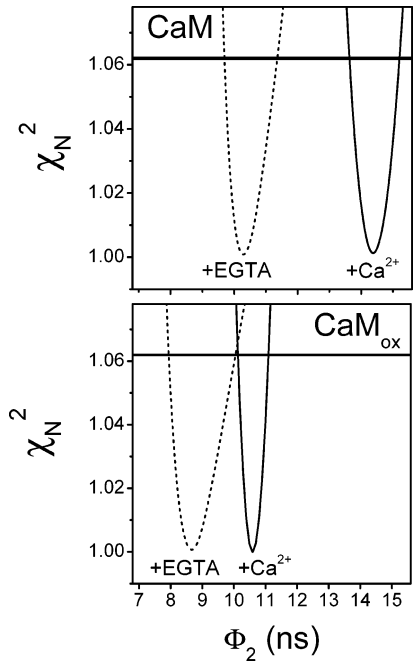

FIGURE 10: Structural uncoupling between opposing domains of calcium-activated CaM following methionine oxidation. Depiction of error surfaces for the rotational dynamics of CaM (top) and CaM_{ox} (bottom) for apo-CaM (dotted line) and following calcium activation (solid line). Normalized χ_N^2 values were determined from nonlinear least-squares fits to the data following the incremental adjustment of the rotational correlation times (φ_2), which were measured from nonlinear least-squares fits to the data depicted in Figure 9. All other fitting parameters were allowed to vary, providing a conservative estimate of possible errors in the calculated rate of motion. The horizontal line at $\chi_N^2 = 1.062$ corresponds to the *F*-statistic, which represents one standard deviation relative to the best fit to the data. Experimental conditions are as described in the legend of Figure 9.

with the formation of a stable three-dimensional binding pocket in the amino-terminal domain, irrespective of methionine oxidation. This structural transition, in which helix A becomes immobilized, functions to couple the amino- and carboxyl-terminal domains in unoxidized CaM (Figure 11). Upon methionine oxidation, the tertiary structure of the amino-terminal domain is altered such that the conformational coupling between the opposing domains that is normally associated with calcium activation is disrupted. The latter result is consistent with prior measurements that suggested a functional and structural role for the oxidation of Met^{144} or Met^{145} in the structural uncoupling between the opposing domains of CaM and the associated functional inactivation of the plasma membrane Ca-ATPase (*15*, *20*, *21*, *31*).

DISCUSSION

Summary of Results. To identify the mechanisms underlying the stabilization of the plasma membrane Ca-ATPase in an inactive conformation upon binding fully oxidized CaM, we have used an engineered CaM that permits the selective and rigid attachment of FlAsH to helix A (Figure 1). Oxidation selectively disrupts the calcium-dependent structural coupling between opposing domains of CaM, without affecting the calcium-dependent immobilization of helix A associated with the formation of the high-affinity binding cleft (Figures 9 and 10 and Table 2). The protein fold is maintained upon oxidation, with minimal changes in the structure of helix A following calcium activation (Figures 3 and 5). Rather, structural rearrangements of interhelical contacts occur to modify the binding cleft for target protein binding, which is apparent from increases in solvent accessibility (Figures 7 and 8), resulting in an enhanced binding affinity between the amino-terminal domain of oxidized CaM and the CaM-binding sequence of the plasma membrane Ca-ATPase (Figure 6).

Calcium Activation and Target Protein Binding. Helix A functions as part of a conformational switch that senses calcium binding to mediate interdomain structural changes associated with the activation of CaM (*9*). Calcium binding is cooperative; initial occupancy of C-terminal domain sites induces structural changes within the amino-terminal domain associated with calcium activation (*47*, *54*−*58*). The structural coupling between the opposing domains of CaM is mediated by the enhanced helical content between Met^{76} and Ser^{81}, which functions to structurally couple helices D and E (*59*−*62*). Thus, the structural coupling between the opposing domains is mediated through the central sequence, and involves the stabilization of calcium-dependent structural interactions between helices H and E in the carboxyl-terminal domain and helices A and D in the amino-terminal domain (*9*, *24*, *29*, *47*, *61*, *63*) (Figure 11). Thus, prior to calcium binding, there are large amplitude helical motions that effectively prevent the formation of a binding cleft; the calcium-dependent stabilization of interhelical contacts favors a defined conformation that permits target protein binding (*7*). These results corroborate models in which calcium activation favors a subset of conformations that expose high-affinity binding sites (*64*). In the case of many target proteins, including the plasma membrane Ca-ATPase, binding of CaM occurs in a sequential manner; upon association with the binding cleft in the C-terminal domain, the N-terminal domain collapses around the target peptide to induce enzyme activation (*11*−*13*). Critical to this binding mechanism is the calcium-dependent stabilization of high-affinity binding clefts in both the carboxyl- and amino-terminal domains of CaM. Association of the C-terminal domain promotes the disruption of the helical content associated with the sequence containing Met^{76}−Ser^{81} to permit the structural collapse of the opposing domains around the linear binding sequence of many CaM-dependent enzymes (*11*, *65*−*67*). Thus, the calcium-dependent stabilization of individual helices within each binding domain to form a binding cleft and the extended structure of calcium-activated calmodulin are both necessary to promote the efficient and ordered binding of the opposing domains of calmodulin to activate target proteins, including the plasma membrane Ca-ATPase (*10*, *68*, *69*).

Methionine Oxidation and CaM Structure. Oxidation of methionines to their corresponding methionine sulfoxides functions to destabilize the structure of CaM, and may contribute to the formation of protein aggregates and diminished levels of CaM present in aging brain (*21*, *46*, *70*, *71*). The functional consequences of oxidizing Met^{144} and Met^{145} with respect to the ability to activate the plasma membrane Ca-ATPase are the same as that observed upon oxidation of all nine methionines (*20*, *21*), suggesting that the majority of methionines have a minimal effect on binding affinity or the induction of structural changes associated with

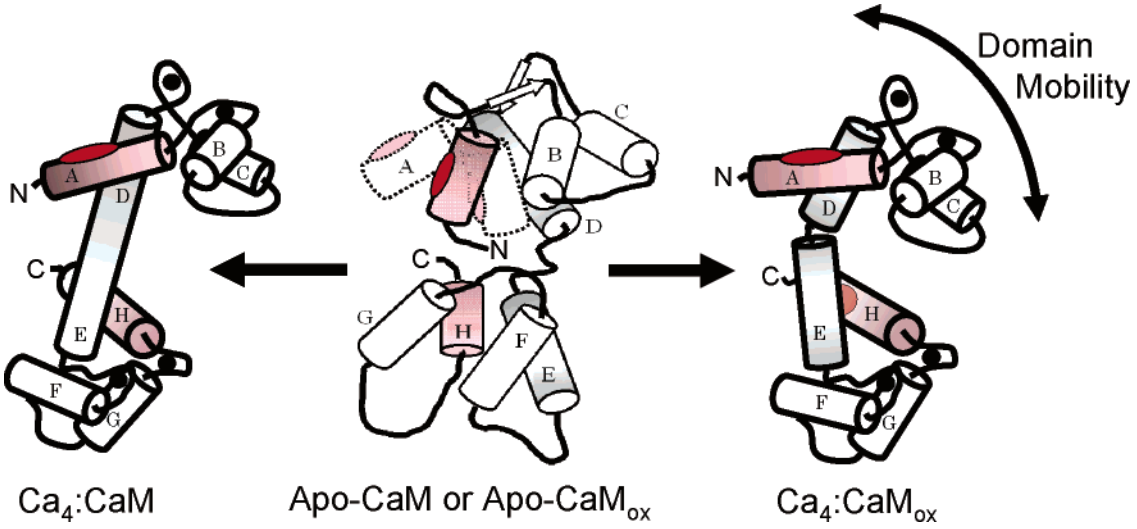

FIGURE 11: Model depicting how methionine oxidation modulates calcium-dependent structural coupling between opposing domains of CaM. FlAsH (red oval) bound to helix A (pink cylinder) in the amino-terminal domain undergoes large amplitude rigid body motions in apo-CaM, which are unaffected upon oxidation of all nine methionines. Calcium activation (black circles) stabilizes the interaction between helix A and helix D (gray shaded cylinders), resulting in the formation of a target peptide binding pocket in the amino-terminal domain. It is suggested that calcium binding to high-affinity sites in the carboxyl-terminal domain induces similar stabilizing interactions between helix H (pink cylinder) and helix E (gray shaded cylinders) that induce the formation of a stable interdomain helix connecting the opposing domains of wild-type (unoxidized) CaM. Upon methionine oxidation, functionally sensitive methionines (i.e., Met^{144} and Met^{145}) in helix H destabilize the interhelical interaction between helix H and helix E, depicted as the appearance of an exposed binding site (light pink circle) (*20*, *21*), resulting in a less stable interdomain interaction through helices D and E connecting the opposing domains of CaM.

target protein activation. Consistent with these results, we find that the tertiary structures of apo- and calcium-activated CaM are very similar irrespective of methionine oxidation (Tables 1 and 2). In all cases, the amplitude and rates associated with the independent motion of helix A (i.e., φ_1) and the rotational dynamics of the amino-terminal domain (i.e., φ_2) are unchanged by methionine oxidation in apo-CaM. These results are in contrast to those of Haiech and coworkers, who found that following oxidation of all nine methionines the apo state is unfolded with essentially random secondary structure (*46*). However, these latter measurements were made following precipitation of CaM with trichloroacetic acid, consistent with a diminished refolding ability of oxidized CaM, and the associated tendency to form aggregates (*17*). Following calcium activation, one observes a similar immobilization of helix A irrespective of methionine oxidation; however, following oxidation, the overall rotational dynamics (i.e., φ_2) are essentially the same irrespective of calcium activation (Figure 10). These latter results are consistent with earlier measurements that indicated oxidation of Met^{144} and Met^{145} results in the structural uncoupling of the opposing domains of calcium-activated CaM. Under these conditions, the amino-terminal domain of CaM binds to the CaM-binding sequence of the plasma membrane Ca-ATPase in a nonproductive conformation that functions to lock the enzyme in a less active conformation.

Methionine Oxidation as a Regulatory Mechanism. During normal biological aging, multiple methionines in CaM are oxidized, serving as a conformational switch to modulate the activation of target proteins and cellular energy utilization (*19*). Given that methionine sulfoxide reductases exist in all cells that function to reduce oxidized methionines (*72*), it is evident that the reversible oxidation of methionines in CaM functions as part of a regulatory circuit to modulate intracellular metabolism in response to conditions of oxidative stress. Indeed, sequence differences near the carboxyl terminus of CaM isoforms modulate the functional sensitivity to oxidative stress (*31*). In this respect, the oxidation of Met^{144} or Met^{145} near the carboxyl terminus functions to destabilize the central helical structure of calcium-activated CaM, resulting in the independent rotational dynamics of the opposing domains of CaM. Under these conditions, the amino-terminal domain of CaM_{ox} is able to associate in an altered conformation to stabilize a nonproductive conformation of the Ca-ATPase with reduced transport activity. Critical to the ability of oxidized CaM to function as an inhibitor of the Ca-ATPase and other target proteins is the retention of the amino-terminal domain switching mechanism, which involves the calcium-dependent immobilization of helix A and exposure of the target protein binding cleft (Figure 9 and Table 2). Thus, the sensitivity of CaM to oxidation permits the downregulation of Ca-ATPase and other target protein activities to slow metabolism and the associated generation of reactive oxygen species associated with the damage of a wide range of proteins.

Conclusions. In summary, oxidation selectively modifies the calcium-bound state of CaM, resulting in the structural uncoupling between the opposing globular domains in CaM with minimal alterations in the calcium-dependent formation of a stable peptide binding cleft that is associated with the immobilization of helix A. These measurements provide evidence for an important role for the structural coupling between the opposing domains of CaM in defining productive binding interactions, and suggest a regulatory mechanism that couples methionine oxidation at selected sites to global conformational changes that modify the function of target proteins. This redox-dependent regulation of CaM function is suggested to underlie adaptive cellular responses to oxidative stress, permitting the rapid reduction of ATP utilization and metabolic flux through the inhibition of CaM-dependent target enzymes.

REFERENCES

1. Yap, K. L., Kim, J., Truong, K., Sherman, M., Yuan, T., and Ikura, M. (2000) Calmodulin target database, *J. Struct. Funct. Genomics 1*, 8−14.
2. Squier, T. C., and Bigelow, D. J. (2000) Protein oxidation and age-dependent alterations in calcium homeostasis, *Front. Biosci. 5*, 1−23.
3. Wang, H., and Storm, D. R. (2003) Calcium-regulated adenylyl cyclases: Cross-talk and plasticity in central nervous system, *Mol. Pharmacol. 63*, 463−468.
4. Fournier, V., Leclerc, P., Cormier, N., and Bailey, J. L. (2003) Implication of calmodulin-dependent phosphodiesterase type 1 during bovine sperm capacitation, *J. Androl. 24*, 104−112.
5. LaPorte, D. C., Wierman, B. M., and Storm, D. R. (1980) Calcium-induced exposure of a hydrophobic surface on calmodulin, *Biochemistry 19*, 3814−3819.
6. Chou, J. J., Li, S., Klee, C. B., and Bax, A. (2001) Solution structure of Ca^{2+}-calmodulin reveals flexible hand-like properties of its domains, *Nat. Struct. Biol. 8*, 990−997.
7. Goto, K., Toyama, A., Takeuchi, H., Takayama, K., Saito, T., Iwamoto, M., Yeh, J. Z., and Narahashi, T. (2004) Ca^{2+} bindings sites in calmodulin and troponin C alter interhelical angle movements, *FEBS Lett. 561*, 51−57.
8. Yang, C., Jas, G. S., and Kuczera, K. (2004) Structure, dynamics and interaction with kinase targets: Computer simulations of calmodulin, *Biochim. Biophys. Acta 1697*, 289−300.
9. Chen, B., Mayer, M. U., Markille, L.-M., Stenoien, D. L., and Squier, T. C. (2005) Dynamic motion of helix A in the amino-terminal domain of calmodulin is stabilized upon calcium activation, *Biochemistry 44*, 905−914.
10. Persechini, A., McMillan, K., and Leaky, P. (1994) Activation of myosin light chain kinase and nitric oxide synthase activities by calmodulin fragments, *J. Biol. Chem. 23*, 16148−16154.
11. Crivici, A., and Ikura, M (1995) Molecular and structural basis of target recognition by calmodulin, *Annu. Rev. Biophys. Biomol. Struct. 24*, 85−116.
12. Ehrhardt, M. R., Urbauer, J. L., and Wand, A. J. (1995) The energetics and dynamics of molecular recognition by calmodulin, *Biochemistry 34*, 2731−2738.
13. Sun, H., and Squier, T. C. (2000) Ordered and cooperative binding of opposing globular domains of calmodulin to the plasma membrane Ca-ATPase, *J. Biol. Chem. 275*, 1731−1738.
14. Kranz, J. K., Flynn, P. F., Fuentes, E. J., and Wand, A. J. (2002) Dissection of the pathway of molecular recognition by calmodulin, *Biochemistry 41*, 2599−2608.
15. Yao, Y., Yin, D., Jas, G., Kuczera, K., Williams, T. D., Schöneich, Ch., and Squier, T. C. (1996) Oxidative modification of a carboxyl-terminal vicinal methionine in calmodulin by hydrogen peroxide inhibits calmodulin-dependent activation of the plasma membrane Ca-ATPase, *Biochemistry 35*, 2767−2789.
16. Gao, J., Yin, D. H., Yao, Y., Sun, H., Qin, Z., Schöneich, C., Williams, T. D., and Squier, T. C. (1998) Progressive decline in the ability of calmodulin isolated from aged brain to activate the plasma membrane Ca-ATPase, *Biochemistry 37*, 9536−9548.
17. Gao, J., Yin, D., Yao, Y., Sun, H., Qin, Z., Schöneich, Ch., Williams, T. D., and Squier, T. C. (1998) Loss of conformational stability in calmodulin upon methionine oxidation, *Biophys. J. 74*, 1115−1134.
18. Toda, T., Morimasa, T., Kobayashi, S., Nomura, K., Hatozaki, T., and Hirota, M. (2003) A proteomic approach to determination of the significance of protein oxidation in the ageing of mouse hipposcampus, *Appl. Genomics Proteomics 2*, 43−50.
19. Bigelow, D. J., and Squier, T. C. (2004) Redox modulation of cellular signaling and metabolism through reversible oxidation of methionine sensors in calcium regulatory proteins, *Biochim. Biophys. Acta* (in press).
20. Bartlett, R. K., Bieber-Urbauer, R. J., Anbanandam, A., Smallwood, H. S., Urbauer, J. L., and Squier, T. C. (2003) Oxidation of Met^{144} and Met^{145} in calmodulin blocks calmodulin dependent activation of the plasma membrane Ca-ATPase, *Biochemistry 42*, 3231−3238.
21. Gao, J., Yao, Y., and Squier, T. C. (2001) Oxidatively modified calmodulin binds to the plasma membrane Ca-ATPase in a nonproductive and conformationally disordered complex, *Biophys. J. 80*, 1791−1801.
22. Yao, Y., Gao, J., and Squier, T. C. (1996) Dynamic structure of the calmodulin-binding domain of the plasma membrane Ca-ATPase in native erythrocyte ghost membranes, *Biochemistry 35*, 12015−12028.
23. Osborn, K. D., Bartlett, R. K., Mandal, A., Zaidi, A., Bieber Urbauer, R. J., Urbauer, J. L., Galeva, N., Williams, T. D., and Johnson, C. K. (2004) Single-molecule dynamics reveal an altered conformation for the autoinhibitory domain of plasma membrane Ca^{2+}-ATPase bound to oxidatively modified calmodulin, *Biochemistry 43*, 12937−12944.
24. Sun, H., Yin, D., and Squier, T. C. (1999) Calcium-dependent structural coupling between opposing globular domains of calmodulin involves the central helix, *Biochemistry 38*, 12266−12279.
25. Grimaud, R., Ezraty, B., Mitchell, J. K., Lafitte, D., Briand, C., Derrick, P. J., and Barras, F. (2001) Repair of oxidized proteins. Identification of a new methionine sulfoxide reductase, *J. Biol. Chem. 276*, 48915−48920.
26. Montgomery, H. J., Bartlett, R., Perdicakis, B., Jervis, E., Squier, T. C., and Guillemette, J. G. (2003) Activation of constitutive nitric oxide synthases by oxidized calmodulin mutants, *Biochemistry 42*, 7759−7768
27. Adams, S. R., Campbell, R. E., Gross, L. A., Martin, B. R., Walkup, G. K., Yao, Y., Liopis, J., and Tsien, R. Y. (2002) New biarsenical ligands are tetracysteine motifs for protein labeling in vitro and vivo: Synthesis and biological application, *J. Am. Chem. Soc. 124*, 6063−6075.
28. Strasburg, G. M., Hogan, M., Birmachu, W., Thomas, D. D., and Louis, C. F. (1988) Site-specific derivatives of wheat germ calmodulin. Interactions with troponin and sarcoplasmic reticulum, *J. Biol. Chem. 263*, 542−548.
29. Sun, H., Yin, D., Coffeen, L. A., Shea, M. A., and Squier, T. C. (2001) Mutation of Tyr^{138} disrupts the structural coupling between the opposing domains in vertebrate calmodulin, *Biochemistry 40*, 9605−9617.
30. Klee, C. B., and Vanaman, T. C. (1982) Calmodulin, *Adv. Protein Chem. 35*, 213−321.
31. Yin, D., Kuczera, K., and Squier, T. C. (2000) The sensitivity of carboxyl-terminal methionines in calmodulin isoforms to oxidation by H_2O_2 modulates the ability to activate the plasma membrane Ca-ATPase, *Chem. Res. Toxicol. 13*, 103−110.
32. Nelson, D. P., and Kiesow, L. A. (1972) Enthalpy of decomposition of hydrogen peroxide by catalase at 25 °C (with molar extinction coefficients of H_2O_2 solutions in the UV), *Anal. Biochem. 49*, 474−478.
33. Laemmli, U. K. (1970) Cleavage of structural proteins during the assembly of the head of bacteriophage T4, *Nature 227*, 680−685.
34. Ferrington, D. A., Sun, H., Murray, K. K., Costa, J., Williams, T. D., Bigelow, D. J., and Squier, T. C. (2001) Selective degradation of oxidized calmodulin by the 20 S proteasome, *J. Biol. Chem. 276*, 937−943.
35. Lakowicz, J. R. (1999) in *Principles of Fluorescence Spectroscopy*, 2nd ed., Kluwer Academic/Plenum Publishers, New York.
36. Chapman, E. R., Alexander, K., Vorherr, T., Carafoli, E., and Storm, D. R. (1992) Fluorescence energy transfer analysis of calmodulin-peptide complexes, *Biochemistry 31*, 12819−12825.
37. Yao, Y., and Squier, T. C. (1996) Variable conformation and dynamics of calmodulin complexed with peptides derived from the autoinhibitory domains of target proteins, *Biochemistry 35*, 6815−6827.
38. Pedigo, S., and Shea, M. A. (1995) Discontinuous equilibrium titrations of cooperative calcium binding to calmodulin monitored by 1-D ^{1}H-nuclear magnetic resonance spectroscopy, *Biochemistry 34*, 10676−10689.
39. Gratton, E., and Limkeman, M (1983) A continuously variable frequency cross-correlation phase fluorometer with picosecond resolution, *Biophys. J. 44*, 315−324.
40. Lakowicz, J. R., and Maliwal, B. (1985) Construction and performance of a variable-frequency phase-modulation fluorometer, *Biophys. Chem. 21*, 61−78.
41. Bevington, P. R. (1969) in *Data Reduction and Error Analysis for the Physical Sciences*, McGraw-Hill, New York.
42. Hunter, G. W., and Squier, T. C. (1998) Phospholipid acyl chain rotational dynamics are independent of headgroup structure in unilamellar vesicles containing binary mixtures of dioleoylphosphatidylcholine and dioleoyl-phosphatidylethanolamine, *Biochim. Biophys. Acta 1415*, 63−76.
43. Weber, G. (1981) Resolution of the fluorescence lifetimes in a heterogeneous system by phase and modulation measurements, *J. Phys. Chem. 85*, 949−953.

44. Klee, C. B., Crouch, T. H., and Krinks, M. H. (1979) Calcineurin: A calcium- and calmodulin-binding protein of the nervous system, *Proc. Natl. Acad. Sci. U.S.A. 76*, 6270−6273.
45. Zhang, M., Li, M., Wang, J. H., and Vogel, H. J. (1994) The effect of Met→Leu mutations on calmodulin's ability to activate cyclic nucleotide phosphodiesterase, *J. Biol. Chem. 269*, 15546−15552.
46. Lafitte, D., Tsvetkov, P. O., Devred, F., Toci, R., Barras, F., Briand, C., Makarov, A. A., and Haiech, J. (2002) Cation binding mode of fully oxidized calmodulin explained by the unfolding of the apostate, *Biochim. Biophys. Acta 1600*, 105−110.
47. Faga, L. A., Sorensen, B. R., VanScyoc, W. S., and Shea, M. A. (2003) Basic interdomain boundary residues in calmodulin decrease calcium affinity of sites I and II by stabilizing helix-helix interactions, *Proteins 50*, 381−391.
48. Kinosita, K., Jr., Ishiwata, S., Yoshimura, H., Asai, H., and Ikegami, A. (1984) Submicrosecond and microsecond rotational motions of myosin head in solution and in myosin synthetic filaments as revealed by time-resolved optical anisotropy decay measurements, *Biochemistry 23*, 5963−5975.
49. Prochniewicz, E., Zhang, Q., Howard, E. C., and Thomas, D. D. (1996) Microsecond rotational dynamics of actin: Spectroscopic detection and theoretical simulation, *J. Mol. Biol. 255*, 446−457.
50. Sabbert, D., Engelbrecht, S., and Junge, W. (1997) Functional and idling rotatory motion within F1-ATPase, *Proc. Natl. Acad. Sci. U.S.A. 94*, 4401−4405.
51. Cantor, C. R., and Schimmel, P. R. (1980) *Biophysical Chemistry, Part II: Techniques for the study of biological structure and function*, p 461, W. H. Freeman and Co., San Francisco.
52. Garcia de la Torre, J., Huertas, M. L., and Carrasco, B. (2000) Calculation of hydrodynamic properties of globular proteins from their atomic-level structure, *Biophys. J. 78*, 719−730.
53. Beechem, J. M., Gratton, E., Ameloot, M., Knutson, J. R., and Brand, L. (1991) The global analysis of fluorescence intensity and anisotropy decay data: Second generation theory and programs, in *Topics in Fluorescence Spectroscopy* (Lakowicz, J. R., Ed.) pp 241−305, Plenum Press, New York.
54. Crouch, T. H., and Klee, C. B. (1980) Positive cooperative binding of calcium to bovine brain calmodulin, *Biochemistry 19*, 3692−3698.
55. Yao, Y., Schöneich, C., and Squier, T. C. (1994) Resolution of structural changes associated with calcium activation of calmodulin using frequency domain fluorescence spectroscopy, *Biochemistry 33*, 7797−7810.
56. Shea, M. A., Verhoeven, A. S., and Pedigo, S. (1996) Calcium-induced interactions of calmodulin domains revealed by quantitative thrombin footprinting of Arg37 and Arg106, *Biochemistry 35*, 2943−2957.
57. VanScyoc, W. S., and Shea, M. A. (2001) Phenyalanine fluorescence studies of calcium binding to N-domain fragments of *Paramecium* calmodulin mutants show increased calcium affinity correlates with increased disorder, *Protein Sci. 10*, 1758−1768.
58. VanScyoc, W. S., Sorensen, B. R., Rusinova, E., Laws, W. R., Ross, J. B. A., and Shea, M. A. (2002) Calcium binding to calmodulin mutants monitored by domain-specific intrinsic phenyalanine and tyrosine fluorescence, *Biophys. J. 83*, 2767−2780.
59. Ikura, M., Spera, S., Barbato, G., Kay, L. E., Krinks, M., and Bax, A. (1991) Secondary structure and side-chain ^{1}H and ^{13}C resonance assignments of calmodulin in solution by heteronuclear multidimensional NMR spectroscopy, *Biochemistry 30*, 9216−9228.
60. Kuboniwa, H., Tjandra, N., Grzesiek, S., Ren, H., Klee, C. B., and Bax, A. (1995) Solution structure of calcium-free calmodulin, *Nat. Struct. Biol. 2*, 768−776.
61. Qin, Z., and Squier, T. C. (2001) Calcium-dependent stabilization of the central sequence between Met^{76} and Ser^{81} in vertebrate calmodulin, *Biophys. J. 81*, 2908−2918.
62. Chang, S. L., Szabo, A., and Tjandra, N. (2003) Temperature dependence of domain motions of calmodulin probed by NMR relaxation at multiple fields, *J. Am. Chem. Soc. 125*, 11379−11384.
63. Sorensen, B. R., Faga, L. A., Hultman, R., and Shea, M. A. (2002) An interdomain linker increases the thermostability and decreases the calcium affinity of the calmodulin N-domain, *Biochemistry 41*, 15−20.
64. Vigil, D., Gallagher, S. C., Trewhella, J., and Garcia, A. E. (2001) Functional dynamics of the hydrophobic cleft in the N-domain of calmodulin, *Biophys. J. 80*, 2082−2092.
65. Ikura, M., Clore, G. M., Gronenborn, A. M., Zhu, G., Klee, C. B., and Bax, A. (1992) Solution structure of calmodulin-target peptide complex by multidimensional NMR, *Science 256*, 632−638.
66. Meador, W. E., Means, A. R., and Quiocho, F. A. (1992) Target enzyme recognition by calmodulin: 2.4 Å structure of a calmodulin-peptide complex, *Science 257*, 1251−1255.
67. Meador, W. E., Means, A. R., and Quiocho, F. A. (1993) Modulation of calmodulin plasticity in molecular recognition on the basis of X-ray structure, *Science 262*, 1718−1721.
68. Yin, D., Sun, H., Ferrington, D. A., and Squier, T. C. (2000) Closer proximity between opposing domains of vertebrate calmodulin following deletion of Met(145)-Lys(148), *Biochemistry 39*, 10255−10268.
69. Sun, H., and Squier, T. C. (2000) Ordered and cooperative binding of opposing globular domains of calmodulin to the plasma membrane Ca-ATPase, *J. Biol. Chem. 275*, 1731−1738.
70. Squier, T. C. (2001) Oxidative stress and protein aggregation during biological aging, *Exp. Gerontol. 36*, 1539−1550.
71. Lu, T., Pan, Y., Kao, S.-Y., Li, C., Kohane, I., Chan, J., and Yankner, B. A. (2004) Gene regulation and DNA damage in the ageing human brain, *Nature 429*, 883−891.
72. Stadtman, E. R., Moskovitz, J., Berlett, B. S., and Levine, R. L. (2002) Cyclic oxidation and reduction of protein methionine residues is an important antioxidant mechanism, *Mol. Cell. Biochem. 234−235*, 3−9.
73. Chattopadhyaya, R., Mendor, W. E., Means, A. R., and Quiocho, F. A. (1992) Calmodulin structure refined at 1.7 Å resolution, *J. Mol. Biol. 228*, 1177−1192.
74. Jencks, W. P. (1969) *Catalysis in Chemistry and Enzymology*, pp 564−565, McGraw-Hill, New York.
75. Laidler, K. J. (1987) in *Topics in Chemical Kinetics*, 3rd ed., p 22, Harper and Row Publishers, New York.
76. van Boom, S. S. G. E., Chen, B. W., Teuben, J. M., and Reedijk, J. (1999) Platinum-thioether bonds can be reverted by guanine-N7 bonds in $Pt(dien)^{2+}$ model adducts, *Inorg. Chem. 38*, 1450−1455.

BI0474113